Tellus (1986), *38B*, 364–374

Non-spherical particles in the antarctic polar stratosphere—increase in particulate content and stratospheric water vapor budget

By YASUNOBU IWASAKA, *Water Research Institute, Nagoya University, Chikusa-ku, Nagoya 464, Japan*

(Manuscript received October 21, 1985; in final form May 26, 1986)

ABSTRACT

The back-scattering coefficient and depolarization ratio of antarctic stratospheric aerosols were observed by a lidar at Syowa Station (69°00′S, 39°35′E) in 1983 in order to understand the nature of polar stratospheric aerosols. Balloon measurement was also made on 3 June to obtain the number concentration of the particles. The balloon data showed a large concentration of particles with radius larger than 0.15 μm (15 particles/cm^3 in the lower stratosphere) and a size distribution which was rich in smaller size particles ($N(r > 0.15\ \mu m)/N(r > 0.25\ \mu m) = 12 \sim 80$, where $N(r > 0.15\ \mu m)$ and $N(r > 0.25\ \mu m)$ are the number concentrations of particles with radius larger than 0.15 μm and 0.25 μm, respectively). During early June, the back-scattering coefficient rapidly increased, but the depolarization ratio was at a low level, at most 0.15. After mid-June, the depolarization ratio increased as the winter progressed, and this suggests that most of the stratospheric particles had non-spherical shapes (possibly ice crystal particles) in mid-winter.

The lidar measurement showed that the stratospheric particles layer was transported downward at the rate of 0.8 mm/s during winter. The mass of water transported from the stratosphere to the troposphere is estimated to be about 5×10^7 ton per winter season if we assume that the settling rate of the layer is due to gravitational sedimentation of ice crystal particles. If it is due to downward air motion carrying smaller crystals, this is reduced to 5×10^4 tons.

1. Introduction

Stanford (1973) suggested that the antarctic stratosphere acted as possible sink of stratospheric water vapor through the "freeze-out" effect, since temperatures in the winter Antarctic lower stratosphere often reached as low as −90°C and put a restriction on the amount of water vapor that could be held by the air of the lower stratosphere. Recently McCormick et al. (1982, 1985) showed, on the basis of SAM II satellite measurements, that the volume of polar stratospheric particulate matter increased as the temperature decreased. Lidar measurements at Antarctica also revealed that the opacity of the antarctic stratospheric aerosol layer was very enhanced during winter (Iwasaka, 1985; Iwasaka et al., 1985a). These observations showed that the content of particulate matter increased under cold stratospheric conditions, but it is not known whether the increase of particulate matter is mostly due to mass increase of background particles (growth) or due to number density increase (nucleation). In addition, it is uncertain whether the particles in the polar winter stratosphere are sulfuric acid droplets or not.

Thermodynamic studies on the aerosol particles existing in the very cold polar stratosphere (Steele et al., 1983) suggested the possibility that active transformation of pre-existing aerosol particles from sulfuric acid droplets to ice crystal particles occurred. The growth of these ice crystals through deposition is an essential factor controlling the increase in particulate matter in the polar winter stratosphere.

During the winter of 1983, the total intensity

and the depolarization ratio of back-scattered light from the stratospheric aerosol were measured using a lidar at Sowa Station (69°00′S, 39°35′E) to investigate the change of particle shape.

One purpose of the present work is to show that new results of these lidar measurements suggested the existence of non-spherical particles in the winter antarctic stratosphere. A further purpose is to discuss the effect of Aitken particle growth on the winter increase in particle content and the effect of the winter enhancement of the antarctic stratospheric aerosol layer on the global budget of stratospheric water vapor.

2. Lidar measurements

In Table 1, the main characteristics of the lidar used here are summarized. The detailed specification of this system were described elsewhere (Iwasaka et al., 1985b) and an outline is given below. The lidar system consists of a 694 nm pulse ruby laser, 50 cm ϕ telescope, dual 100 channels photon-counters, A scope, A/D converter processing. Lidar measurements on the stratosphere have been made since April 1983 at Showa Station (69°00′S, 39°35′E), Antarctica as a part of the international project "Antarctic Middle Atmosphere (1982–1986)".

The scattering ratio, $R(Z)$, is defined as follows (e.g., Russell et al., 1976),

$$R(Z) = [B_1(Z) + B_2(Z)]/B_1(Z), \quad (1)$$

where $B_1(Z)$ and $B_2(Z)$ are the molecular and particulate back-scattering coefficients, respectively, at altitude Z. The usual matching of the lidar signal containing both molecular and particulate back-scattering with the profile of molecular back-scattering was made using the radiosonde measurements which were routinely made at Showa Station. The mixing ratio of

Table 1. *Main characteristics of the laser radar system*

Transmitter	
Laser output	>1 J/pulse (694 nm)
	>0.3 J/pulse (347 nm)
Laser pulse width	40 ns
Repetition rate	60 ppm (max)
Laser beam divergence	1.6 mrad
Transmitter optics	Galilean telescope (×4)
Transmitter beam divergence	0.5 mrad (30 mm diameter)
Receiver	
Receiver optics	Cassegrain telescope
Receiver diameter	500 mm
F-number	*F*/4.0
Receiver field of view	0.5–2.0 mrad
Transmitter/receiver mount	
Vertical direction only (fixed type)	
Detection system	
3-channel detection (typical confirmation)	
A-channel PMT R-943-02	347 nm ± 1.3 nm
B-channel PMT R-943-02	694 nm ± 0.5 nm
C-channel PMT R-1333	694 nm ± 0.5 nm
PMT R-1332	347 nm ± 1.3 nm
Signal processing	
Analog method	
A-D converter	8-bit resolution
	Sampling speed 50 ns (max)
Photon counting method	
Multichannel counter	8-bit resolution
	Range resolution 100 m (min)
Data processing	
CAMAC data logging system with minicomputer (Melcom 70/10)	

particulate matter is estimated by,

$$R(Z) - 1 = B_2(Z)/B_1(Z). \quad (2)$$

When linearly polarized laser light is incident on a unit volume of air, the back-scatter fraction from atmospheric molecules is slightly depolarized due to the anisotropy of air molecules. Non-spherical aerosol particles also produce some depolarization. Irregular volcanic ash and ice crystal particles produce large amounts of depolarization of back-scatter light (e.g., Pal and Carswell, 1976). Measurement of the depolarization ratio of back-scattered light, $D(Z)$, should therefore be very useful in detecting the presence of non-spherical particles such as ice crystals in the polar stratosphere. It is defined by,

$$D(Z) = P_\perp(Z)/P_\parallel(Z), \quad (3)$$

where $P_\perp(Z)$ and $P_\parallel(Z)$ are the received back-scatter power polarized in planes perpendicular and parallel, respectively, to the transmitted laser beam which is linearly polarized.

3. Results

In Fig. 1, some typical profiles of the scattering ratio are shown, together with the correspondent temperature distribution. The scattering profile is maximum during winter and scattering layers are thicker as compared to those occurring during other seasons.

The vertically integrated back-scattering coefficient in the stratosphere is given by,

$$I = \int_{\Delta Z} B_2(Z)\,dZ, \quad (4)$$

where ΔZ is the height range from the base of the layer to the top. We chose the tropopause instead of the bottom of the layer when tropospheric clouds disturbed the base of the layer near the tropopause. The integrate I can be recognized as the parameter corresponding to the column mass concentration of particulate matter although this is not fully quantitative (Northam et al., 1974; Hofmann et al., 1983). The variation of I is shown in Fig. 2. The integrated back-scattering

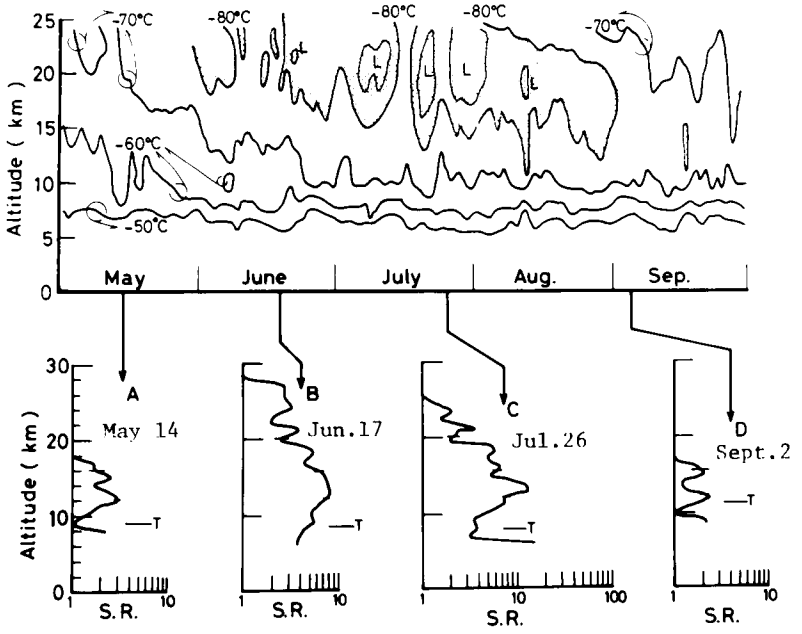

Fig. 1. Temperature distribution and scattering ratio profiles measured at Syowa Stations (69°00′S, 39°35′E) in 1983. The region with temperature lower than −80°C is shaded, and the regions labeled "L" show the areas with lower than −85°C. The aerosol layer top is very high and the scattering ratio of the layer peak large in winter.

coefficient reaches its maximum in winter, 1983. Similar events were also seen by the SAM II satellite (McCormick et al., 1982, 1985). Therefore, the enhancement of the antarctic stratospheric aerosol layer during winter is not an event peculiar to winter, 1983, but occurs regularly every winter. Here, this phenomena will be referred to as the winter enhancement of the antarctic stratospheric aerosol layer.

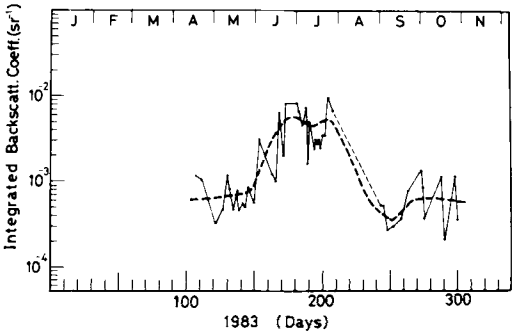

Fig. 2. Vertically integrated back-scatter coefficients of aerosols (see text). The large value in winter appears to correspond to the low temperature of the winter stratosphere.

The correspondence of depolarization ratio to back-scattering coefficient is shown in Fig. 3a and b. All dots in figures indicate half-monthly averaged values. Fig. 3a shows the correspondence in the height range from the base of the layer to 100 mb, and Fig. 3b in the height range from 100 mb to 50 mb.

4. Discussion

4.1. Increase in particulate matter content

The lidar results shown in Figs. 1 and 2 suggest an increase in the content of particulate matter during winter, and confirm the results obtained by SAM II satellite measurements (McCormick et al., 1982, 1985). The results in Fig. 3 indicate that the depolarization ratio also increased to relatively large values during winter. Such large values, as far as we know, have not been measured in the low- and mid-latitudes stratosphere. This suggests that stratospheric aerosols

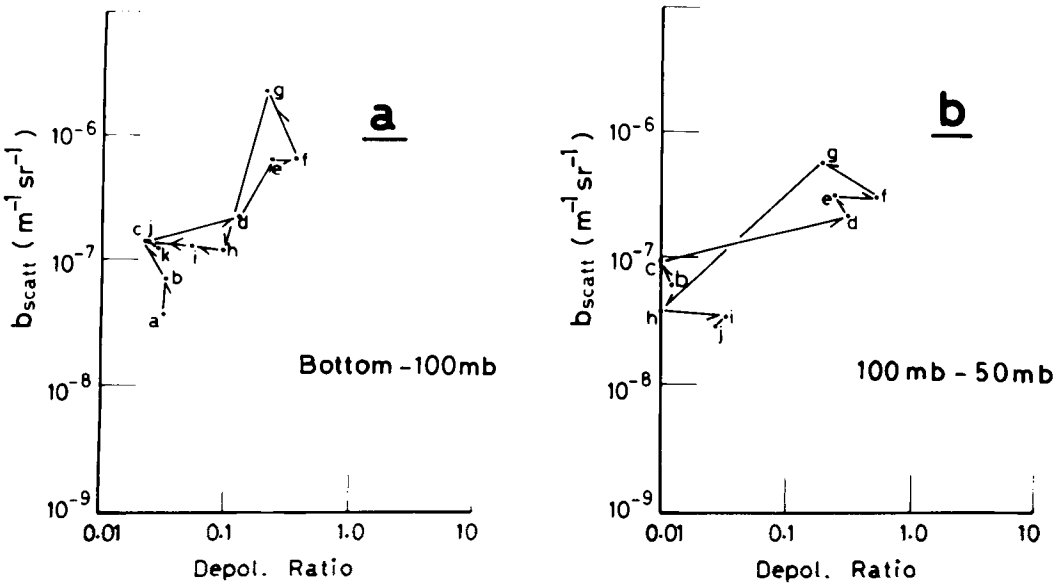

Fig. 3. Correspondence of depolarization ratio (Depol. Ratio) to back-scatter coefficient (b_{scatt}). (a) Shows the average value of measurements obtained form the layer bottom to 100 mb; (b) those from 100 mb to 50 mb, respectively. Dots are half-monthly averaged values as follows: a, April 16–30, 1983; b, May 1–15, 1983; c, May 16–31, 1983; d, June 1–15, 1983; e, June 16–30, 1983; f, July 1–15, 1983; g, July 16–31, 1983; h, September 1–15, 1983; i, September 16–30, 1983; j, October 1–15, 1983; k, October 16–31, 1983.

are essentially composed of sulfuric acid and have spherical shapes (droplets). Ice clouds such as cirrus frequently show large values exceeding 0.5 (e.g., Pal and Carswell, 1976). The measurements obtained during the period of fully developed enhancement, June 30, is shown in Fig. 4. This profile shows that the depolarization ratio of the mid-winter antarctic stratospheric aerosol layer

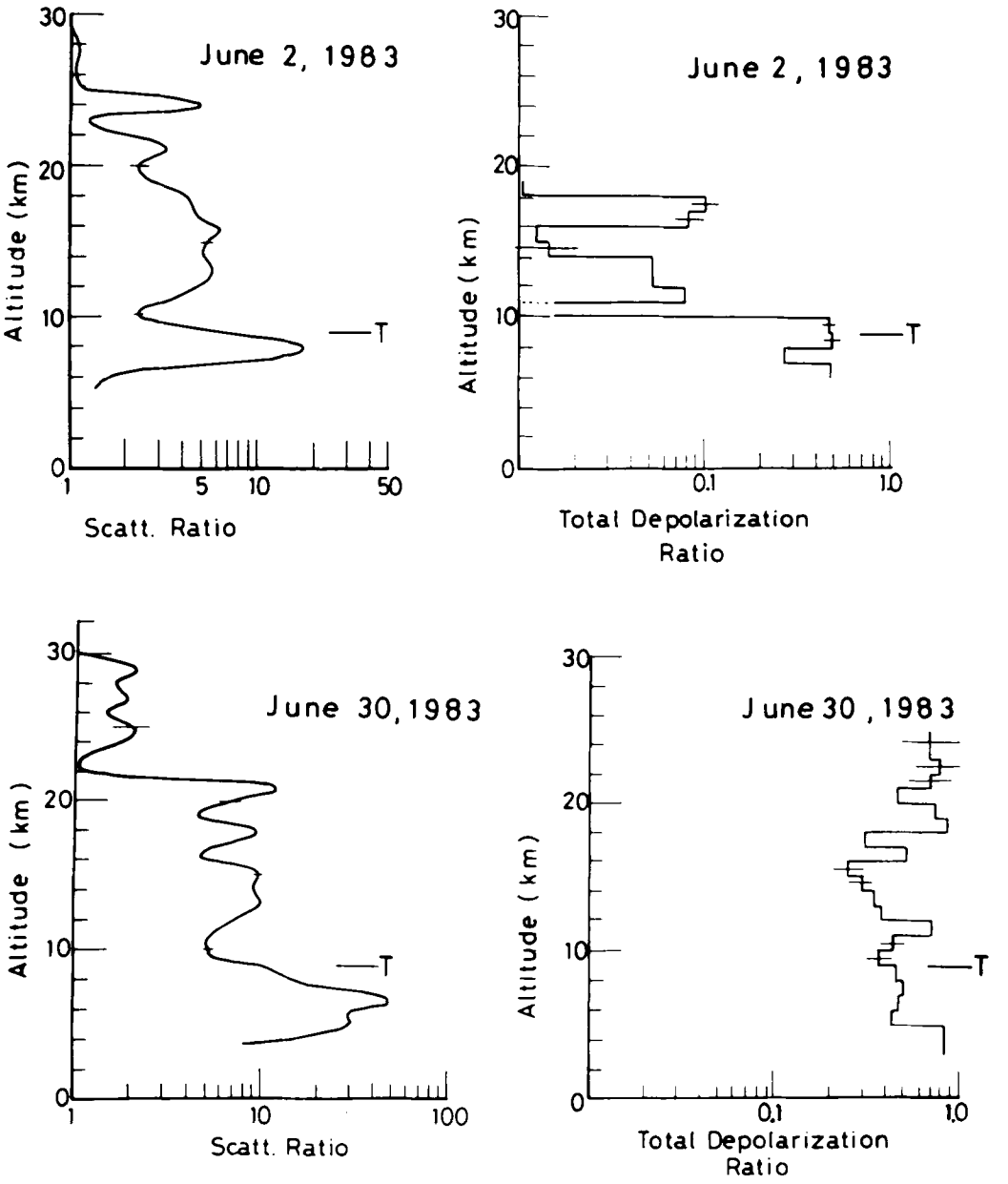

Fig. 4. Comparison of lidar measurements in winter. The scattering ratio becomes noticeably large in winter, but the depolarization ratio is at low levels in early winter, 1983. Curves of June 2, 1983 are typical examples in early winter, and curves of June 30 those showing features of the mid-winter aerosol layer.

becomes comparable to that due to ice crystal in cirrus clouds.

Steele et al. (1983) presented the hypothesis that the increase in particulate matter was due to the increase in mass of individual particles. According to them, these particles grow from pre-existing sulfuric acid droplets through the dilution and the freezing of fully dilute droplets. Very little growth takes place until the temperature drops to the freezing point of pure ice or the saturation point of water. The lidar measurements will be described later; the possibly increased particle number concentration may also be important in increasing the particulate matter content of the polar winter stratosphere.

4.2. *Aerosol content increase during the onset of the winter enhancement*

It should be noticed that the lidar measurements showed a large scattering ratio but not a large depolarization ratio in early winter. Typical samples are compared in Fig. 4. The scattering ratio of June 2 in Fig. 4 showed a large mixing ratio of aerosol particles (about 30–50 times larger than the levels measured in mid-latitudes during calm periods). However, the depolarization ratio is not so large that we can definitely conclude the existence of non-spherical particles. The same features were found in measurements on June 12. After June 15, the depolarization ratio rapidly increased and showed a good correspondence with the large back-scattering coefficient (see Fig. 3).

Fortunately, the size distribution and number concentration of particles with size larger than 0.15 μm were observed by a balloon-borne particle counter at Syowa Station on June 2, 1983 (Morita, 1984, pers. comm.). These results revealed that above the tropopause, the number concentration of particles with radius >0.15 μm was quite high, above 15 particles/cm^3. Previous observations, mostly during summer, showed that the stratospheric aerosol number concentration was 1 particle/cm^3 at most during the calm stratospheric periods (e.g., Rosen et al., 1975), and 7 particles/cm^3 during the disturbed periods (Hofmann and Rosen, 1984). This difference may therefore indicate a seasonal component in number concentration, although a possible contribution from the El Chichon volcanic eruption (Spring 1982, Mexico) cannot be dismissed.

It is expected that most stratospheric particles are composed of sulfuric acid droplets from heteromolecular nucleation with water vapor and sulfuric acid molecules. According to kinetic theory, the rate at which the ith molecule strikes a particle per unit area is given by

$$p_i/\sqrt{2\pi m_i kT}, \tag{3}$$

where p_i is the partial pressure of the ith gas, m_i the mass of the ith molecule, k Boltzmann's constant, and T the atmospheric temperature. Considering the surface area of typical stratospheric aerosols, S, the characteristic time scale of particle growth by collision is given by,

$$\tau_{c,i} = [S \times (P_i/\sqrt{2\pi m_i kT}) \times v_i/V]^{-1}, \tag{4}$$

where v_i and V are the volume of the molecule and aerosol, respectively. The time scales of water vapor molecules ($i=1$) and sulfuric acid molecules ($i=2$) are as follows, assuming that $P_1 = 10^{-4}$ mm Hg, $P_2 = 10^{-13}$ mm Hg, $T = 200$ K, $V = 4.2 \times 10^{-12}$ cm^3, and $S = 10^{-7}$ cm^2 (e.g., Viggiano and Arnold, 1983),

$\tau_{c,1} = 5$ s,

$\tau_{c,2} = 10^9$ s.

It should be noticed that the time scale of temperature variation in the antarctic stratosphere is about 10^6 s and smaller than $\tau_{c,2}$. This means that we can ignore the effect of H_2SO_4 molecule collisions in discussing the winter enhancement.

The particle growth rate, dV/dt, is given by,

$$\frac{dV}{dt} = [\alpha(P_1 - P_{d,1})/\sqrt{2\pi k m_1 T}]\, v_1\, S, \tag{5}$$

where $P_{d,1}$ is the saturation vapor pressure, and α the sticking efficiency (unity is assumed).

The growth time scales of particles with volume V are estimated by,

$$\tau_g(r) = \left[\frac{1}{V}\frac{dV}{dt}\right]^{-1}. \tag{6}$$

This implies that the growth rate of Aitken-size particles is faster than that of large particles. For example, the radii 0.05 and 0.5 μm,

$$\tau_g(0.05\ \mu\text{m})/\tau_g(0.5\ \mu\text{m}) \simeq 10. \tag{7}$$

For extremely small particles, the Kelvin effect is important and therefore the term $(p_1 - p_{d,1})$ in eq. (5) should be modified. Steele and Hamill

(1981) investigated the Kelvin effects on stratospheric aerosol growth. According to them, this effect is important for a temperature of 200 K and for aerosols with size smaller than 0.005 μm. However, for large particles, this effect is negligible.

Steele et al. (1983) and McCormick et al. (1985) suggested that the SAM II measurements were in good agreement with the log-normal size distribution function of background aerosols; total density = 6.3 particles cm^{-3}, mode radius = 0.0725 μm, and $\sigma = 1.86$. According to their estimation, the change of particle size is small up to the water saturation point the frost point.

Considering the temperature measured in early June and the typical stratospheric water vapor content, about 5 ppmv, neither supersaturation of water vapor for ice nor that for water can take place during the set-up stage of the enhancement. The concentration of particles with radius larger than 0.15 μm during this period will be about unity at most if we follow the model of Steele et al. (1983). However, as described above, the particle density was larger than that.

The balloon measurement of June 3 also showed that the particle number ratio $N(r > 0.15\ \mu\text{m})/N(r > 0.25\ \mu\text{m})$, where $N(r > 0.15\ \mu\text{m})$ and $N(r > 0.25\ \mu\text{m})$ are the number concentration of particles with radius $> 0.15\ \mu$m and $> 0.25\ \mu$m, respectively, was 12–80 above the tropopause (Morita, 1984, pers. comm.). The size distribution was far from log-normal, exponential, and ZOLD type. From the large ratio of the particle concentration, it seems likely that there are many particles with radius smaller than 0.15 μm.

Summarizing these facts, we can conclude that during the early stage of the enhancement, particles formed with radius larger than 0.15 μm were not ice crystal particles. Consequently, this provides a large contribution to the increase in the particle content during the early phase.

4.3. *Ice particle formation*

As the temperature decreases in the winter stratosphere, sulfuric acid molecules in aerosols cannot follows the new stratospheric conditions owing to the lack of collision frequency in the time scale of interest. Consequently, the chemical composition of aerosols under the new atmospheric conditions is controlled only by collisions between water vapor molecules and aerosol particles. The necessary condition for growth of aerosol particles is that the water vapor pressure of molecules exceeds the local saturation vapor pressure. The Clausuis-Clapeyron equation is given by,

$$\frac{dp_{d,1}}{P_{d,1}} = \frac{L_v m_1}{k} \frac{dT}{T^2}, \tag{8}$$

where L_v is the latent heat of vaporization. By integration of eq. (8), we find

$$T = \frac{T_0}{1 - [kT_0/(L_v m_1)] \ln(p_{d,1}/p_{0,1})}, \tag{9}$$

where $p_{0,1}$ is the known saturation vapor pressure at temperature T_0. The frost point temperature for water vapor mixing ratios of 5 ppmv and 10 ppmv was estimated using $L_v = 2.8 \times 10^{10}$ ergs/g, $T_0 = 273$ K, $p_{0,1} = 6.11 \times 10^3$ dyn/cm^2.

The frost point temperature of water vapor (curves g and h), the saturation temperature of water vapor on sulfuric acid solution (c, d for sulfuric acid solution 75% weight, and e, f for 50% solution) and saturation temperature of sulfuric acid vapor (a, b for 75% solution) are shown in Fig. 5. The temperatures are estimated on the basis of the results of Ayers et al. (1980), and by Gmitro and Vermeulen (1964).

The freezing point of sulfuric acid solution is a function of the weight percentage of H_2SO_4. According to Gable et al. (1950), pure ice freezes out from sulfuric acid solution with about 40% H_2SO_4 weight when the temperature drops below -73°C. If the weight percentage of H_2SO_4 decreases further through dilution, the freeze-out temperature increases. For example, the freeze-out point becomes about -35°C for a 30% sulfuric acid droplet. Thus, the decreases of stratospheric temperature cause active dilution of the sulfuric acid droplet and enlarges the difference between atmospheric temperature and the freeze-out point of ice from the droplet.

In Fig. 6, the vapor pressure of water over sulfuric acid solutions (10%, 30%, 40%, and 50% weight) are shown. The water vapor pressure for pure water is the same as that for a 10% sulfuric acid solution (Steele et al., 1983; Gmitro and Vermeulen, 1964; McDonald, 1965). Region "a" indicates the range of the temperature measured in the height range 125 to 50 mb from June 15 to July 30, 1983 at Syowa Station. Region "b" shows

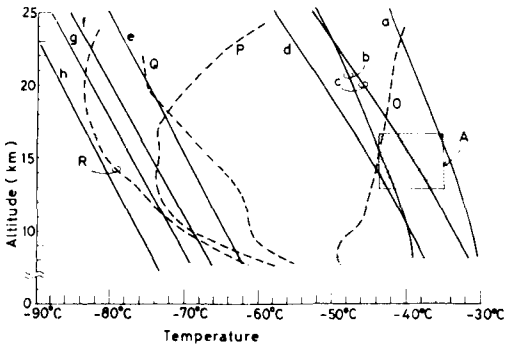

Fig. 5. Comparison of atmospheric temperatures and saturation (or frost) point temperatures of water vapor and sulfuric acid vapor. Curves O, P, Q, and R are the atmospheric temperatures which are half-monthly averages on the basis of radiosonde measurements at Syowa Station, and show typical feature of each season: O, February 1–15, 1983 (summer); P, September 16–30, 1983 (spring); Q, May 16–31, 1983 (fall); R, July 1–15, 1983 (winter). Curves (a) and (b) are saturation point temperatures of sulfuric acid vapor with 0.2 pptv and 0.1 pptv mixing ratio for sulfuric acid solution of 75% weight. Curves (a) and (d) are saturation point temperatures of water of 10 ppmv and 5 ppmv, respectively, for a sulfuric acid solution of 75% weight, and curves (e) and (f) are for sulfuric acid solution of 50% weight. Curves (h) and (g) are frost point temperatures of water vapor with mixing ratios 10 ppmv and 5 ppmv, respectively. In winter, the atmospheric temperature frequently falls to a value lower than the frost point temperature, (h). The shaded area (A) indicates the region in which typical stratospheric aerosol particles of about 75% sulfuric acid can exist.

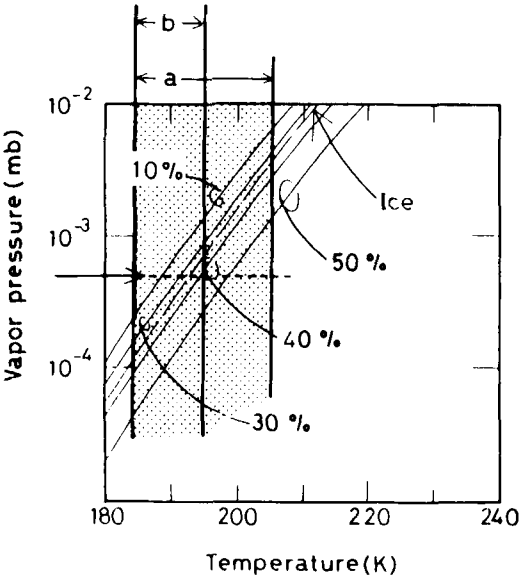

Fig. 6. Water vapor pressures for sulfuric acid solutions; 10%, 30%, 40%, and 50%, weight. Vapor pressure on ice is indicated by a dotted line. The shaded area (a) shows the temperature range measured form 125 mb to 50 mb height (Syowa Station, June 15–July 30). Area (b) indicates the range in which depolarization ratios larger than 0.5 was observed. The arrow indicates the water vapor pressure, corresponding to a water vapor mixing ratio of 5 ppmv at 100 mb height.

the temperature range at which the large depolarization ratio (larger than 0.5) was measured. Most measurements were in the region "b" during this period; 77% for 125–50 mb, and 85% for 100–50 mb.

Atmospheric temperature profiles showing the characteristics of each season are compared in Fig. 5 on the basis of the routine sonde sounding at Syowa Station. The temperature distribution *R*, which is an averaged value during the period from July 1 to July 15, was lower than the frost point temperature *g* for the water vapor mixing ratio of 10 ppmv, and comparable to the frost point temperature for a mixing ratio of about 6 ppmv. In summer, the stratospheric temperature O is in the range where sulfuric acid droplets with 75% weight are in equilibrium with the surrounding atmosphere. When the temperature decreases rapidly, supersaturation occurs for water vapor and sulfuric acid vapor. However, as described before, it is reasonable to consider that only water vapor molecules can condense rapidly onto the aerosol particles.

Composition of aerosol droplets can change from about 75% to about 10% through dilution since the temperature drops frequently below −85°C during winter in the height range from 125 to 50 mb if we assume the mixing ratio of water vapor is 5 to 10 ppmv (the case of 100 mb height is shown by an arrow in Fig. 6). Droplets with about 30% weight or below will be supercooled by more than 40°C, and these particles will be frozen if we follow Hallet and Lewis (1967). Owing to subsequent temperature drop, particles can be sufficiently diluted to be treated as ice particles, and rapid growth through deposition can occur when the temperature decreases below the frost point.

As pure ice occupies the major proportion of

particle volume, it is reasonable to assume that the particle shape depends on the freeze-out ice. Usually, ice crystals in the atmosphere have non-spherical shapes, and a large depolarization ratio can be expected. Thuman and Robinson (1954) observed that over 90% of ice particles in fogs near Fairbanks, Alaska at temperature below −38°C, were approximately spherical shape (these are named "droxtals"). Kumai (1966) also found spherical ice crystals of 2 μm to 15 μm diameter formed at around −40°C. Kobayashi (1965) grew ice crystals from water vapor between −40 and −90°C using a small diffusion cold box. In this range of temperature, the basic shape of the crystals was prism like. Long prisms and whiskers occurred at low supersaturation between −45 and −50°C. Pyramidal faces appeared at the ends of prisms between −50 and −90°C. Ohtake (1970) noted that "droxtals" included 20-faced bi-pyramids on short prisms and also 14-faceted bi-pyramid crystals. These crystals seem to be similar to those which Kobayashi (1965) grew in the laboratory. From the observations and the experiments, it seems likely that "droxtals" and faceted crystals present a low-temperature quasi-stable state.

In view of Kobayashi's experiments (1956) on the shapes of ice crystals at low temperatures, it might be expected that stratospheric ice particles which are just a few μm in diameter, will develop pyramidal faces (Hobbs, 1974). The large depolarization ratio measured in the winter antarctic stratosphere (although the crystal shapes of ice cannot be estimated directly from the measurements) show the existence of non-spherical particles which are speculated to be ice crystals.

In Fig. 7, the region where atmospheric temperature is lower than the frost point temperature, is illustrated; the upper limit for the mixing ratio of water vapor is 10 ppmv and the lower 5 ppmv. If we assume a water vapor mixing ratio of 6 ppmv in the winter antarctic stratosphere, we find general agreement between estimations and the observations at Syowa Station.

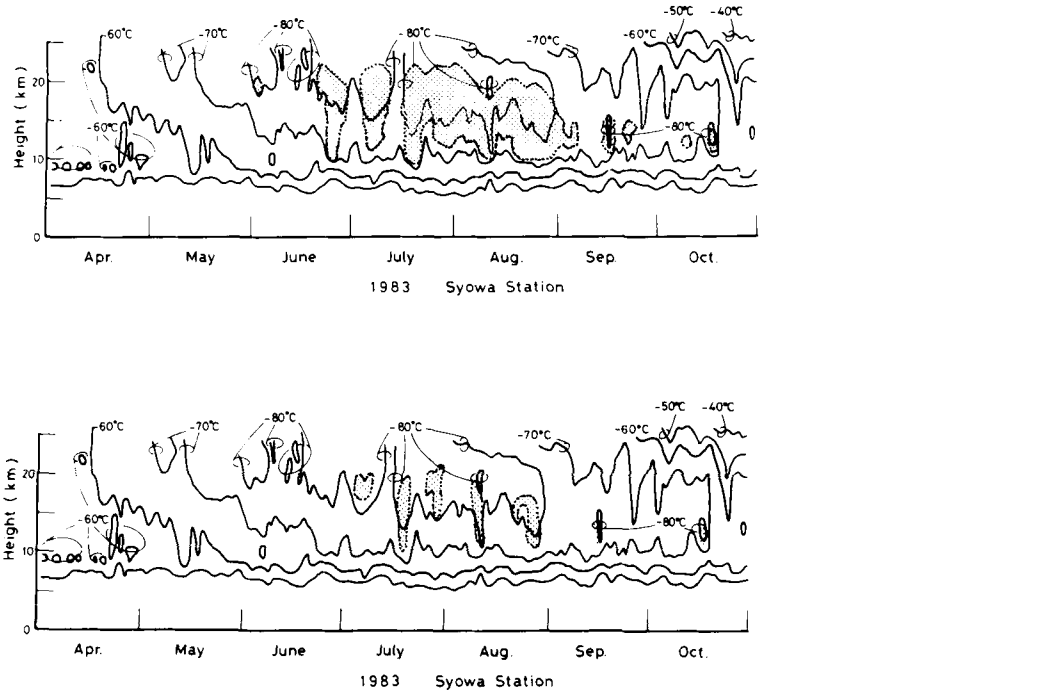

Fig. 7. Freezing of water droplets can occur in the shaded area. The upper figure is for a water vapor mixing ratio of 10 ppmv, and the lower for 5 ppmv. The temperature distribution is given on the basis of routine radiosonde measurements at Syowa Station.

4.4. Possible effect of the winter antarctic stratosphere on the global budget of stratospheric water vapor

It is worth noticing that the height of the layer center descended at the rate of about 0.8 mm/s in the winter season, and this motion was closely related to the descent of the cold region (Iwasaka, 1986). McCormick et al. (1985) pointed out that the same motion with a descending rate of 0.77 mm/s was also found in the antarctic stratosphere and suggested that this motion was related to the large-scale air motion in the winter stratosphere.

The interpretation of this motion is not yet certain, but the descending motion found by lidar and satellite, is an important factor controlling the transport of particles, if this motion means substantial movement of particles.

If we assume the descending motion is due to air motion, and an average particle size of about 0.2 μm, the flux of water due to this is about 4×10^{-14} g cm^{-2} s^{-1}. For the assumption that particle sedimentation causes this descending motion, the particle size should be 2 μm or larger and the flux about 4×10^{-11} g cm^{-2} s^{-1}. The horizontal scale of events is unknown. Considering that the increase of particulate matter is highly correlated to the cold temperature field in winter, the area of enhancement of stratospheric aerosol layer, is about 17×10^{16} cm^2 (the polar area at latitudes higher than 70°S). The lidar measurements show that the duration of an event is about 3 months to 4 months. Assuming a constant flux at the tropopause level, we estimate the mass of water transported from the stratosphere to the troposphere to be 5×10^4 and 5×10^7 ton per winter for displacement due to subsidence and sedimentation, respectively. The mass of water transported by the global-scale air motion is of the order 10^8 tons per year (e.g., Ellsaesser, 1974, 1983). The present rough estimates suggest the importance of particle growth and transportation during the antarctic winter for the global budget of stratospheric water vapor.

5. Summary and conclusions

Summarizing the lidar and balloon measurements on stratospheric aerosols at Syowa Station (69°00′S, 39°35′E), we can mention the following.

(1) During winter, particulate matter content is extremely enhanced.
(2) Increase in particle number concentration (nucleation) possibly contributed to the winter enhancement of stratospheric aerosols during the onset stage of the enhancement.
(3) During the main stage of the enhancement, the depolarization ratio of particles was very large, but was low during the onset stage.
(4) Most of the aerosol particles are transferred to ice particles during the main stage of the enhancement. Growth of ice particles through deposition contributes to the winter enhancement.
(5) If the descending motion of the particle layer measured during winter is due to particles sedimentation, the antarctic winter stratosphere is a possible sink for stratospheric water vapor.

The studies described in this paper are based on the measurements of a single station during a period of one year. Further investigation is necessary to understand the nature of polar stratospheric aerosols. Better information on the size distribution and composition of particles is badly needed. Simultaneous measurements of water vapor and aerosol particles are also needed. It is important to determine the mechanism of the descending motion of the aerosol layer in order to assess the effect of the winter enhancement of the aerosol layer on the global budget of the stratospheric water vapor. Information on the horizontal scale of the enhancement is also essential.

6. Acknowledgements

It is a pleasure to acknowledge continuous encouragement from Professor T. Hirasawa, National Institute of Polar Research. Members of 24th Japanese Antarctic Research Expedition (leader: Professor S. Mae, Hokkaido University) assisted the author during the lidar measurements. The engineering staffs of the Nippon Electric Company gave technical support, which is gratefully acknowledged.

REFERENCES

Ayers, G. P., Gillett, R. W. and Gras, J. L. 1980. On the vapor pressure of sulfate acid. *Geophys. Res. Lett. 7*, 433–436.

Gable, C. M., Betz, H. F. and Maron, S. M. 1950. Phase equilibria of the system sulfur trioxide-water. *J. Am. Chem. Soc. 72*, 1445–1448.

Ellsaesser, H. W. 1974. Water budget of the stratosphere, Third CIAP conference, Rep. DOT-TSC-OST-74-15, U.S. Dep. Transp., 273–283.

Ellsaesser, H. W. 1983. Stratospheric water vapor. *J. Geophys. Res. 88*, 3897–3906.

Gmitro, J. I. and Vermeulen, T. 1964. Vapor-liquid equilibria for aqueous sulfuric acid. *A.I.Ch.E. J. 10*, 740–746.

Hayashida, S., Kobayashi, A. and Iwasaka, Y. 1984. Lidar measurements of stratospheric aerosol content and depolarization ratios after the eruption of El Chichon volcano: Measurements at Nagoya, Japan. *Geofys. Int. 23-2*, 277–288.

Hallett, J. and Lewis, R. E. J. 1967. Mother-of-pearl clouds. *Weather 22*, 56–65.

Hobbs, P. 1974. *Ice physics*. Clarendon Press, 662 pp.

Hofmann, D. J., Rosen, J. M., Reiter, R. and Jager, H. 1983. Lidar- and balloon-borne particle counter comparisons following recent volcanic eruptions. *J. Geophys. Res. 88*, 3777–3782.

Hofmann, D. J. and Rosen, J. M. 1984. Detection of El Chichon volcanic aerosol in the antarctic stratosphere. *Antarct. J. 16*, 196–199.

Iwasaka, Y. 1985. Lidar measurement of the stratospheric aerosol layer at Syowa Station (69°00′S, 39°35′E), Antarctica. *J. Meteorol. Soc. Japan 63*, 283–287.

Iwasaka, Y., Hirasawa, T. and Fukunishi, H. 1985a. Lidar measurements on the Antarctic stratospheric aerosol layer [I] Winter enhancement. *J. Geomag. Geoelectr. 37*, 1087–1095.

Iwasaka, Y., Itoh, S., Yasuda, M. and Ohtani, H. 1985b. Laser radar system for atmospheric studies at Syowa Station, Antarctica. *NEC Research & Development No. 76*, 44–54.

Iwasaka, Y. 1986. Lidar measurements on the Antarctic stratospheric aerosol layer [II]. The changes of layer height and thickness in winter. *J. Geomag. Geoelectr. 38*, 99–109.

Kobayashi, T. 1965. Vapour growth of ice crystal between −40 and −90°C. *J. Meteorol. Soc. Japan 43*, 359–367.

Kumai, M. 1966. Electron microscopic study of ice-fog and ice-crystal nuclei in Alaska. *J. Meteorol. Soc. Japan 45*, 185–194.

McCormick, M. P., Hamill, P. and Farrukh, U. O. 1985. Characteristics of polar stratospheric clouds as observed by SAM II, SAGE, and lidar. *J. Meteorol. Soc. Japan 63*, 267–276.

McCormick, M. P., Steele, H. M., Hamill, P., Chu, W. P. and Swissler, T. J. 1982. Polar stratospheric cloud sightings by SAM II. *J. Atmos. Sci. 39*, 1387–1397.

Northam, G. B., Rosen J. M., Melfi, S. H., Pepin, T. J., McCormick, M. P., Hofmann, D. J. and Fuller, W. H. 1974. Dustsonde and lidar measurements of stratospheric aerosols: A comparison. *Appl. Opt. 13*, 2416–2421.

Ohtake, T. 1970. Unusual crystal in ice fog. *J. Atmos. Sci. 27*, 509–511.

Pal, S. R. and Carswell, A. I. 1976. Multiple scattering in atmospheric clouds: Lidar observations. *Appl. Opt. 15*, 1990–1995.

Russell, P. B., Viezee, W., Hake, Jr., R.D. and Collis, R. T. H. 1976. Lidar observations of the stratospheric aerosol: California, October 1972–March 1974. *Q.J.R. Meteorol. Soc. 102*, 675–695.

Rosen, J. M., Hofmann, D. J. and Laby, J. 1975. Stratospheric aerosol measurements II: The worldwide distribution. *J. Atmos. Sci. 32*, 1457–1462.

Stanford, J. L. 1973. On the physics of stratospheric (nacreous) cloud formation. *Tellus 25*, 479–482.

Steele, H. M. and Hamill, P. 1981. Effects of temperature and humidity on the growth and optical properties of sulfuric acid-water droplets in the stratosphere. *J. Aerosol Sci. 12*, 517–528.

Steele, H. M., Hamill, P., McCormick, M. P. and Swissler, T. J. 1983. The formation of polar stratospheric cloud. *J. Atmos. Sci. 40*, 2055–2067.

Thuman, W. C. and Robinson, E. 1954. Studies of Alaskan ice-fog particles. *J. Meteorol. 11*, 151–156.

Viggiano, A. A. and Arnold, F. 1983. Stratospheric sulfuric acid vapor: New and update measurements. *J. Geophys. Res. 88*, 1457–1462.